CHEMISTRY
A European Journal

A Journal of
ChemPubSoc Europe

Accepted Article

Title: Carbazole Linked NIR Aza-BODIPY Dyes as Triplet Sensitizers and Photoacoustic Contrast Agents for Deep Tissue Imaging

Authors: Nagaiyan Sekar, Ramaiah D, Yogesh Gawale, Adarsh N., Joseph J, M. Pramanik, and S K Kalva

This manuscript has been accepted after peer review and appears as an Accepted Article online prior to editing, proofing, and formal publication of the final Version of Record (VoR). This work is currently citable by using the Digital Object Identifier (DOI) given below. The VoR will be published online in Early View as soon as possible and may be different to this Accepted Article as a result of editing. Readers should obtain the VoR from the journal website shown below when it is published to ensure accuracy of information. The authors are responsible for the content of this Accepted Article.

To be cited as: *Chem. Eur. J.* 10.1002/chem.201605702

Link to VoR: http://dx.doi.org/10.1002/chem.201605702

Supported by
ACES

WILEY-VCH

10.1002/chem.201605702

WILEY-VCH

Carbazole Linked NIR Aza-BODIPY Dyes as Triplet Sensitizers and Photoacoustic Contrast Agents for Deep Tissue Imaging

Yogesh Gawale[a], Nagappanpillai Adarsh[b], Sandeep Kumar Kalva[c], Joshy Joseph[b], Manojit Pramanik[c]*, Danaboyina Ramaiah[d]* and Nagaiyan Sekar[a]*

Abstract: Four novel *N*-ethylcarbazole linked aza-BODIPY dyes (**8a-b** and **9a-b**) were synthesized and characterized. The presence of *N*-ethylcarbazole moiety shifts their absorption and fluorescence spectra to the near-infrared region, *ca*. 650-730 nm, of electromagnetic spectra. These dyes possess strong molar absorptivity in the range of 3-4 x 10^4 $M^{-1}cm^{-1}$ with low fluorescence quantum yields. The triplet excited state as well as singlet oxygen generation of these dyes were enhanced upon iodination at the core position. The core iodinated dyes **9a-b** showed excellent triplet quantum yield of *ca*. 90% and 75% with singlet oxygen generation efficiency of *ca*. 70% and 60% when compared to the parent dyes. The derivatives **8a**-**b** showed dual absorption profiles in contrast to the dyes **9a**-**b**, which has the characteristic absorption band of the aza-BODIPY dyes. DFT calculations revealed the electron density spread over the iodine and dipyrromethene plane of **9a**-**b**, whereas in **8a**-**b** the electron density distributed on carbazole group as well as dipyrromethene plane of aza-BODIPY. The uniqueness of these aza-BODIPY systems is that they exhibit efficient triplet state quantum yields, high singlet oxygen generation yields and good photostability. Further we explored the photoacoustic (PA) characteristics of these aza-BODIPY dyes, and observed efficient PA signals for **8a** compared to blood serum with *in vitro* deep tissue imaging, thereby confirming its use as a promising photoacoustic contrast agent.

Introduction

There are four major reactive oxygen species (ROS) comprising superoxide ($O_2^{\cdot-}$), hydroxyl radical (·OH), hydrogen peroxide (H_2O_2), and singlet oxygen $O_2(^1\Delta_g)$, but all these species show different level of activity and kinetics. The hydroxyl radical and singlet oxygen are more toxic and acutely lethal compared to superoxide and hydrogen peroxide. The generation of singlet oxygen through photosensitization is one of the most utilized method in recent years.[1] Due to the spin-allowed nature of the reactions, singlet oxygen exhibits high reactivity towards most of the organic molecules and thus it has the ability to interrupt the cellular functions in living organisms. Photodynamic therapy is based on the formation of reactive oxygen species (ROS), specifically singlet oxygen, upon activation of the photosensitizer by light.[2] It damages the biological tissues by subsequent oxidation. Hence, the quantitative generation of singlet oxygen (Φ_Δ) is one of the important requirement of an efficient photosensitizer (PS).[3]

Most of the photosensitizers used for the generation of singlet oxygen comprises of a common cyclic tetrapyrrolic structure, derived from porphyrins. Apart from this several non-porphyrinic systems reported in the literature to serve the purpose of singlet oxygen generation and these include methylene blue, Nile blue, Nile red, Rose bengal, chalcogenopyrylium salts, squaraine dyes etc.[4] However, the drawbacks of such classes of PS are low molar absorption coefficients in the near infra-red (NIR) region and dark toxicity. An ideal PS should possess good stability and should have high absorption in the range of 600-800 nm, below which the light will be absorbed by different tissues and above which it does not provide energy to excite oxygen to its singlet state.[5]

Recently, the chemistry of dipyrromethene ligands and their boron complexes (BODIPY) has attracted much attention due to their favorable photophysical properties such as intense absorption at long wavelength with high molar absorption coefficients (ε>10^4 $M^{-1}cm^{-1}$), moderate to quantitative fluorescence quantum yields and chemical properties, which include tunability through substitution at different positions.[6] Aza-dipyrromethenes and aza-BODIPY dyes were first described several years ago as blue pigments, but now are rapidly emerging as a class with desirable near infrared photophysical properties.[7]

The strong absorption of light in the NIR region has also finds potential application of these dyes as photoacoustic (PA) contrast agent.[8] PA imaging is gaining attention as an emerging deep tissue biomedical imaging modality that incorporates rich optical contrast and high ultrasound resolution. Due to this added advantage, PA imaging finds many applications in breast cancer imaging, brain imaging, tumour angiogenesis, molecular imaging, sentinel lymph node imaging, vascularisation monitoring and so on.[9] Moreover, these contrast agents help in targeted PA imaging and molecular imaging with high contrast and sensitivity.[10]

[a] Y. Gawale, Prof. N. Sekar
Dyestuff Technology Department,
Institute of Chemical Technology,
Matunga, Mumbai, 400 019, India,
n.sekar@ictmumbai.edu.in, nethi.sekar@gmail.com

[b] Dr. N. Adarsh, Dr. J. Joseph
Chemical Sciences and Technology Division
CSIR-National Institute for Interdisciplinary Science and Technology, Thiruvananthapuram - 695 019, Kerala, India

[c] S. K. Kalva, Dr. M. Pramanik
School of Chemical and Biomedical Engineering
Nanyang Technological University
62 Nanyang Drive, Singapore 637459,
manojit@ntu.edu.sg

[d] Dr. D. Ramaiah
CSIR-North East Institute of Science and Technology,
Jorhat 785 006, Assam, India
d.ramaiah@gmail.com

Supporting information for this article is given via a link at the end of the document.

Accepted Manuscript

This article is protected by copyright. All rights reserved.

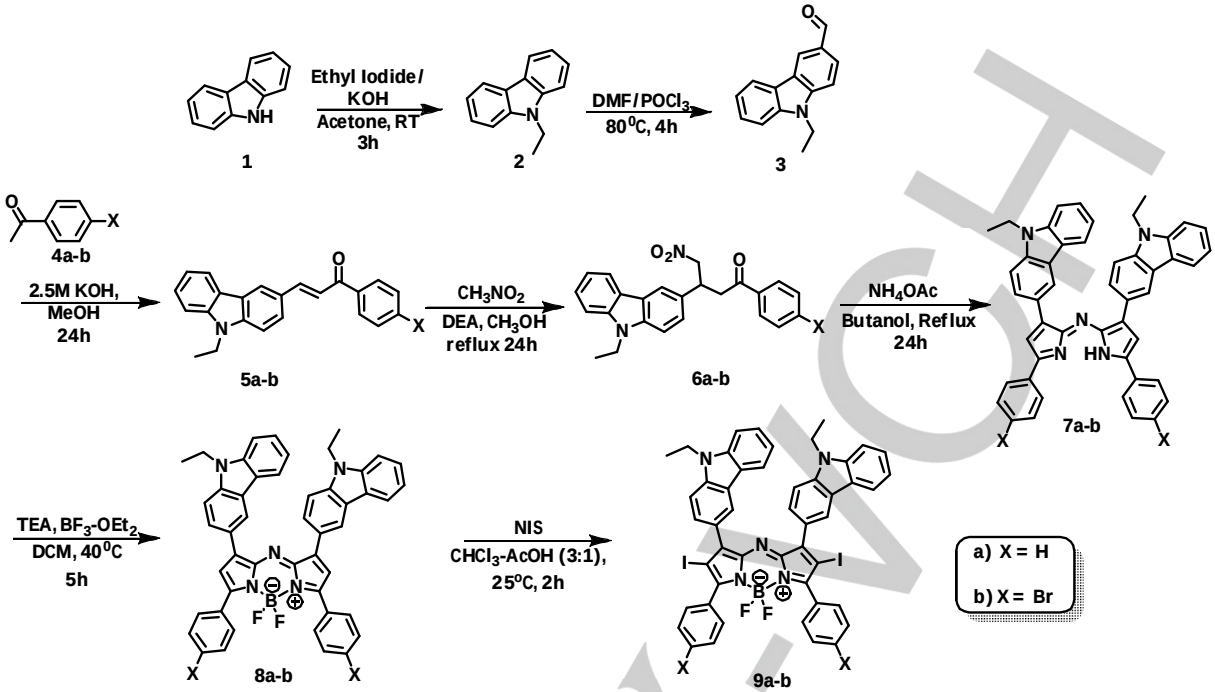

Scheme 1: Synthetic route for the aza-BODIPY dyes **8a-b** and **9a-b**.

Herein, we designed a new series of carbazole linked aza-BODIPY derivatives with an objective of developing new and efficient photosensitizers and photoacoustic imaging agents that exhibit near infrared absorption in the range of *ca.* 600-800 nm. We synthesized a series of the *N*-ethylcarbazole linked aza-BODIPY dyes, characterised and have investigated their photophysical properties, triplet excited state and singlet oxygen generation efficiencies. The photoacoustic characteristics of the dyes were investigated and the derivative, **8a** was found to be efficient for *in vitro* deep tissue imaging application.

Results and Discussion

Synthesis and characterization: The synthetic strategy adopted for the synthesis of *N*-ethylcarbazole linked aza-BODIPY **8a-b** and **9a-b** using different acetophenone derivatives is shown in Scheme 1. The aza-BODIPY derivatives **8a-b** and **9a-b** were synthesized in a facile six step route starting from carbazole **1**. *N*-Ethylation of carbazole by ethyl iodide in acetonitrile yielded **2,** which upon Vilsmeier-Haack formylation gave the corresponding formyl derivative **3,** in good yield. Further, aldol condensation reaction between **3** and the acetophenone derivatives **4a-b** yielded the respective chalcones **5a-b.** The addition of nitromethane to the chalcone in presence of diethylamine gave the adducts **6a-b,** which upon refluxing with ammonium acetate in n-butanol for 20 h gave the corresponding aza-dipyrromethenes **7a-b** as condensation products. The aza-dipyrromethenes **7a-b** were subsequently converted to the targeted aza-BODIPY derivatives **8a-b** (35-40%) by reacting with borontrifluoride diethyletherate and triethylamine at 40°C in dichloromethane for 5 h. The controlled iodination of **9a-b** was carried out by modifying the reported procedures using NIS as the iodinating agent and achieved 60-65% yield.[3a]

Absorption and fluorescence properties: *N*-Ethylcarbazole linked aza-BODIPY dyes, **8a-b** showed very distinct photophysical properties as compared to their iodinated derivatives, **9a-b.** The non-iodinated dyes **8a-b** showed dual absorption in the red region (610-720 nm) and having molar extinction coefficients 3.0 and 3.2 × 10^4 $M^{-1}cm^{-1}$, (Figure S27, Supporting Information) respectively. Interestingly, for the core iodinated aza-BODIPY derivatives **9a-b**, we observed a single absorption profile with a maximum at *ca.* 645-655 nm (Figure 1A S24, Supporting Information), with an enhanced molar absorptivity of *ca.* 3.7 and 4.1 × 10^4 $M^{-1}cm^{-1}$, respectively. All these aza-BODIPY derivatives exhibited good solubility in common organic solvents such as CH_3CN, $CHCl_3$, THF and DMSO.

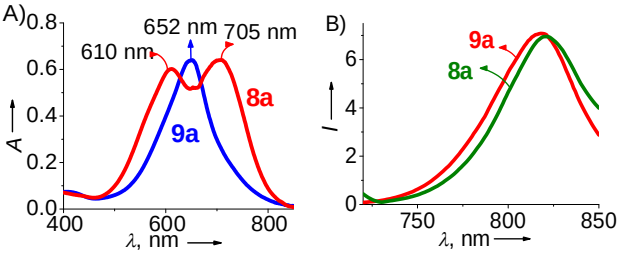

Figure 1: A) Absorption and B) fluorescence spectra of the representative aza-BODIPY derivatives **8a** and **9a** in acetonitrile (20 µM each).

Accepted Manuscript

This article is protected by copyright. All rights reserved.

Table 1. Summary of photophysical, electrochemical and theoretical parameters for the aza-BODIIPY dyes **8a-b** and **9a-b**

Dyes	λ_{abs} (nm)	ε_{max} ($M^{-1}cm^{-1}$)	λ_{em} (nm)	Φ_f[a]	Stokes shift (cm^{-1})	E_{HOMO}		E_{LUMO}		E_{gap}		Triplet and singlet oxygen parameters		
						Experiment	Theory	Experiment	Theory	Experiment	Theory	Φ_T[b]	τ_T[c]	Φ_Δ[d]
8a	705	3.0×10^4	818	0.22	1959.46	-5.322	-5.297	-3.86	-3.381	1.462	1.916	e	e	1
9a	653	3.7×10^4	815	0.03	3067.49	-5.343	-3.583	-3.899	-1.050	1.444	2.533	90	1.15	70
8b	723	3.2×10^4	820	0.03	1636.14	-4.082	-5.324	-2.69	-3.461	1.39	1.863	E	e	1
9b	649	4.1×10^4	830	0.32	3360.13	-4.16	-3.645	-2.67	-1.102	1.48	2.544	75	1.64	61

[a] Absolute quantum yield in % [b] Quantum yield of triplet state, were calculated by using the triplet–triplet energy transfer in % [c] Triplet state lifetime [d] Quantum yeild of singlet oxygen, were quantified through scavenging of $^1O_2$ by DPBF [e] Triplet is not observed in Acetonitrile.

Figure 1B (Figure 26, Supporting Information) shows the emission spectra of the corresponding *N*-ethylcarbazole linked aza-BODIPY derivatives in acetonitrile. The aza-BODIPY derivatives **8a-b** showed emission in the region 815-825 nm with Stokes shifts of 113 nm and 97 nm, respectively. Interestingly, the core iodine substituted aza-BODIPY derivatives **9a-b**, also showed emission maxima in the region 815-830 nm marking large Stokes shifts values of 163 nm and 181 nm, respectively.

Determination of triplet excited state quantum yields: The transient intermediates such as triplet excited states involved in these systems were characterized and quantified through nanosecond laser flash photolysis. The time-resolved transient absorption spectra of the compounds were studied. Figure 2 shows the transient absorption spectra of **9a** in acetonitrile obtained after 355 nm laser excitation (10 ns, 50 mJ/ pulse). For the derivative **9a,** the transient absorption spectra has two peaks at 320 nm and 460 nm with a strong bleach in the region corresponding to its ground state absorption. The transient was characterized as triplet excited state using oxygen quenching experiments as reported previously.[11, 6d] The triplet formed from **9a** within laser pulse, decayed by a first-order process with a lifetime value of 1.15 µs (Inset of Figure 2).

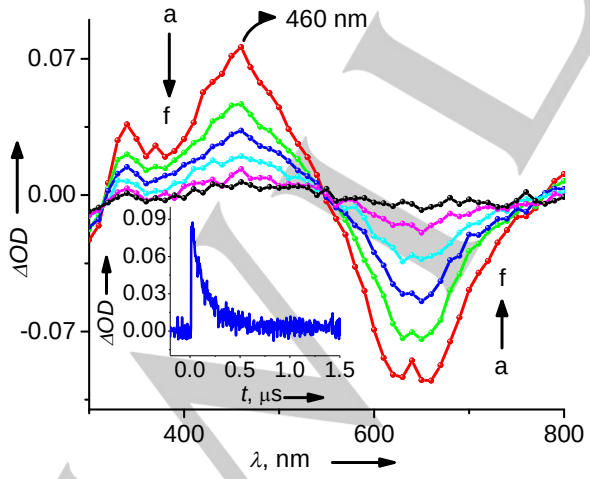

Figure 2: Transient absorption spectra of A) **9a** following 355 nm laser pulse excitation; time-resolved absorption spectra recorded at (a) 0.5, (b) 0.2 (c) 0.1, (d) 0.05, (e) 2 µs. Inset shows the decay of the transient at 460 nm.

In case of dye **9b,** similar transient absorption spectrum observed having bands at 320 nm and 460 nm formed upon the excitation with 355 nm laser (Figure S28, Supporting Information). Triplet quantum yields of **9a** and **9b** derivatives were determined using triplet-triplet energy transfer to *β*-carotene using tris(bipyridyl)ruthenium(II) complex as the reference (Table 1).[7c, 12]

Quantification of singlet oxygen generation: Enhanced triplet quantum yields are favorable for the efficient generation of singlet oxygen and therefore we have examined the singlet oxygen generation efficiency of the derivatives **9a** and **9b** in acetonitrile. Quantum yields of singlet oxygen generation were determined by monitoring the photooxidation of 1,3-diphenylisobenzofuran (DPBF) through absorption spectroscopy.[13] For this, a solution of the aza-BODIPY derivative and DPBF were irradiated using 630 nm long pass over a time period of 0-10 s and the decrease in the absorption band of (~10%) of DPBF at 409 nm was monitored (Figure 3A). Yields for the generation of singlet oxygen were calculated using the standard, Methylene Blue (MB), and by plotting the ΔOD of DPBF against the irradiation time (Figure 3B). The non-iodinated aza-dipyrromethenes **8a** and **8b** showed negligible singlet oxygen generation efficiency.

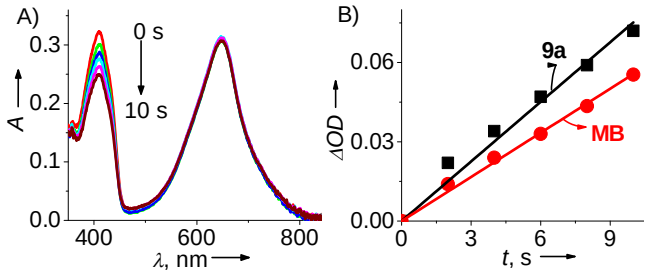

Figure 3: A) Absorption spectra of diphenylisobenzofuran (DPBF) upon irradiation in presence of **9a** from 0 to 10 s (recorded at 2 s interval) in ACN, B) straight line plot between the changes in absorption of DPBF with the irradiation time.

From the previous reports, it is clear that the tuning of singlet oxygen generation efficiencies of the aza-BODIPY derivatives can be achieved by suitably incorporating the heavier halogen atoms such as iodine and bromine at the core as well

This article is protected by copyright. All rights reserved.

as at the peripheral phenyl rings.[3a] We have observed the similar effect for the carbazole linked aza-BODIPY dyes **8a-b** and **9a-b**. The aza-BODIPY derivative, **8a** showed negligible singlet oxygen generation efficiency while a slight improvement was observed with peripheral substitution with bromine as in **8b** (Table 1). On the other hand, a significant enhancement in singlet oxygen generation was observed upon iodination at core position (**9a**). To summarize, the derivatives **9a** and **9b**, having two iodine atoms at the core of the pyrrole exhibited singlet oxygen quantum yield of 70% and 60%, respectively (Figure 3, S29, Supporting Information) when compared to the standard **MB** (Φ_Δ = 52%).[14] The negligible changes in the absorption spectra after irradiating an oxygen saturated solution of these dyes for 2 h, indicates their photostability under these conditions.

Electrochemical properties: We have investigated the oxidation and reduction potentials of **8a-b** and **9a-b** using cyclic voltammetry and square wave voltammetry techniques in acetonitrile using 0.1 M $TBAPF_6$ as the supporting electrolyte. Acetonitrile solutions were purged with N_2 and scanned at a rate of 100 mV s^{-1}.The redox potentials were calculated using the potentials obtained from the square wave voltammograms (Figure S30, Supporting Information). Table 1 lists the calculated HOMO-LUMO energies of the compounds **8a-b** and **9a-b**. It can be seen that unlike ferrocene, which showed single oxidation wave at 0.38 V,[15] all the aza-BODIPY derivatives exhibited two oxidation and two reduction waves in their cyclic voltammograms (CV). Incorporation of the iodo atom at core position of aza-BODIPY **8a** and **8b** has a negative effect on the oxidation potentials (E_{OX}). The dyes **8a** (E_{OX}= 5.322 V) and **8b** (E_{OX}=5.343 V) possess higher oxidation potential as compared to **9a** (E_{OX}= 4.082 V) and **9b** (E_{OX}=4.16 V), by 1.24 V and 1.18 V. This can be attributed to the presence of iodine atom at the core position, which leads to the rigidification of the core and hence the reduction processes become more feasible for the aza-BODIPY **8a** and **8b.** The HOMO values of the aza-BODIPY derivatives increases in the order **8b**<**8a**<**9b**<**9a**.

Frontier molecular orbital energies. The energy levels of the frontier molecular orbitals (FMOs), especially HOMO-1, HOMO, LUMO and their spatial distributions are useful to predict the behavior of the molecules in terms of their electronic structures, photophysical properties, and photostability. Herein we report the contour plots of the HOMO-1, HOMO and LUMO of dyes **8a**, **9a**, **8b** and **9b** in acetonitrile as shown in (Figure 4, S31, Supporting Information). These energy values were calculated by employing B3LYP/6-31G level of theory for aza-BODIPY **8a, 8b, 9a,** and **9b**. These states encompasses a complex orbital contribution, beyond the crude HOMO−LUMO, so that barely considering these two frontier orbitals would not provide accurate energy gap [16, 6f] and hence deviated more compared to the experimental energy gap. HOMO-1 orbital of dye **8a** and **8b** clearly indicate the electron density is situated more on the carbazole ring as compared to the aza-BODIPY core. Whereas, HOMO-1 orbital of dye **9a** and **9b** indicate the whole electron density is situated on pyrrole core towards iodine atom due to its heaviness. In the case of HOMO of dye **8a** and **8b**, the electron density is distributed almost uniformly over the entire chromophore. Interestingly, for the dyes **9a** and **9b**, unlike for dyes **8a** and **8b**, the electron density in HOMO is localized only on the pyrrolic position and the aza-BODIPY core.

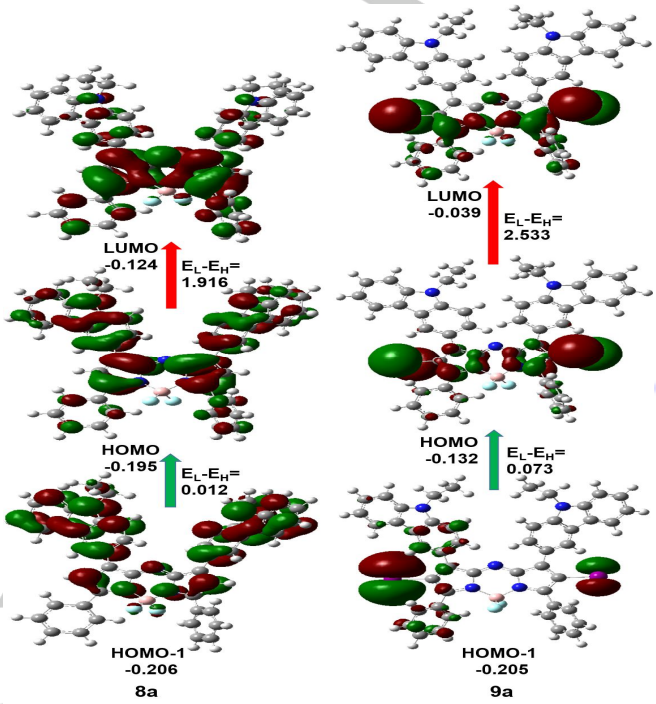

Figure 4: Energy level diagram containing the HOMO-1, HOMO and LUMO levels of **8a and 9a** calculated at B3LYP/6-31g level.

DFT results suggested that iodination at the core position of aza-BODIPY affects the orientation of carbazole group at the peripheral position. The dihedral angle of **8a** (1c-2c-3c-4c) between the carbazole group and dipyrromethene plane is 21^0, whereas the dihedral angle of **9a** increases to 41^0 (Figure 5). Similar observations noticed in case of aza-BODIPY **8b** and **9b,** in which the dihedral angle increased from 20^0 to 41^0.[7i] Hence we have observed reasonable enhancement in band gap of iodinated derivatives **9a** and **9b** as compared to **8a** and **8b.**

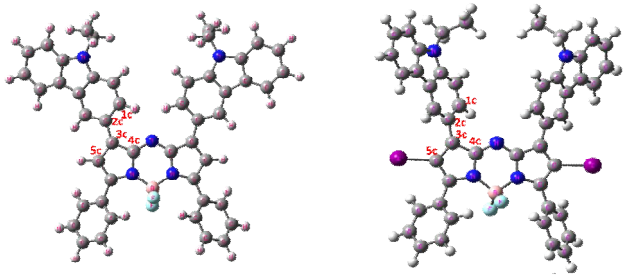

Figure 5. Optimized geometry of **8a** and **9a** at B3LYP/6-31g level.

Photoacoustic spectrum (PAS). According to the Kasha's rule,[17] the non-radiative decay ($S_n \rightarrow S_1$) is responsible for the enhancement in PA signal, followed by the competition between radiative and non-radiative pathways for the S1→S0 transition. An organic material having strong NIR absorption and long-lived S1 excited state (life time of excited state) facilitating excited-state absorption is expected to produce an enhanced PA

Accepted Manuscript

This article is protected by copyright. All rights reserved.

signal.[18] We further attempted to understand the potential of aza-BODIPY dyes as molecular photoacoustic contrast agents in solution as well as in the tissue. We have initially performed the photoacoustic study on the aza-BODIPY dyes (**8a-b**, **9a-b**) in acetonitrile at a concentration of 30 µM. The PA spectra were measured in the wavelength range from *ca*. 670-970 nm with an interval of 5 nm. The PAS of each sample is compared to that of animal blood. Figure 6A (Fig. S32, Supporting Information) shows the PA spectrum of samples **8a-b**, **9a-b** dissolved in acetonitrile with respect to the PA spectrum of blood. Peak to peak normalized PA signal has been calculated at each wavelength.

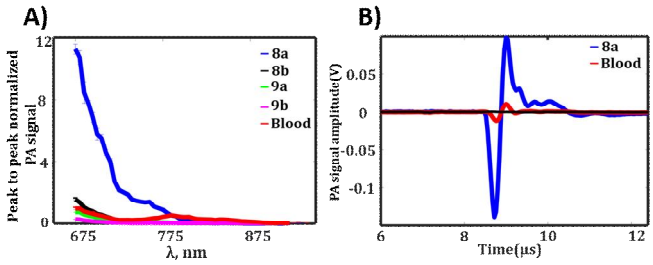

Figure 6: Photoacoustic spectra of aza-BODIPY dyes in acetonitrile (30 uM). (A) PA spectra of **8a**, **8b**, **9a,** and **9b** in solvent ACN compared to that of blood. (B) PA signal comparison of sample 8a in ACN with blood and water (control data) at 675 nm.

The PA signal of dyes **8a** and **8b** are higher than that of blood compared to the rest of the samples at 675 nm. The PA signal of the core iodinated derivatives **9a-b** are much lower than that of blood which may be due to the enhanced intersystem crossing of **9a-b**, that results in the shortening of S1 lifetime. Also the iodo atom at the core position of the aza-BODIPYs **9a** and **9b** push the carbazole group out of plane to a major extent and does not allow taking part in direct conjugation with dipyrromethene ring which may reduce vibrations and thus the thermoelastic expansion in the molecule. The dyes **8a** and **8b**, which are free from the core substitution showed strong PAS signal when compared to blood. These can be attributed to their low intersystem crossing efficiency, which leads to an increase in the singlet excited state life time. The peak to peak PA signal amplitude for the sample **8a** in acetonitrile is found to be 12 times higher than that of blood (Figure 6B), and the signal intensity gets increased upon increasing the concentration of the sample. Therefore, the derivative, **8a** can be used as a promising photoacoustic contrast agent in deep tissue imaging.

Deep tissue photoacoustic imaging. To demonstrate the potential of the aza-BOIDPY derivative, **8a** as a promising PA contrast agent, and to determine its imaging depth, a study was conducted to acquire the PA images of **8a** (in acetonitrile) and blood embedded inside chicken breast tissue (CBT). Two low density polyethylene (LDPE) tubes of 0.38 mm inner diameter were filled with blood and **8a** and placed on layer of CBT as shown in Figure 7A. PA data was acquired using a 2.25 MHz ultrasound transducer (UST) at various depths of *ca*. 1cm and *ca*. 2 cm by stacking layers of CBT one on top of the other (Figure 7B). Figures 7C and 7D show the reconstructed cross-sectional photoacoustic tomography (PAT) images at 1 cm and 2 cm depths, respectively. The signal-to-noise ratio (SNR) at *ca*. 1 cm depth for **8a** is measured to be 53.15 dB and for blood 29.63 dB. Notably at *ca*. 2 cm depth the SNR for **8a** is found to be 42.23 dB whereas the blood tube was not visible at all. The PA signal for the aza-BODIPY derivative, **8a** is clearly seen even at the depth of 2 cm. Hence, the aza-BODIPY dye, **8a** can be used as a promising photoacoustic contrast agent that produces rich contrast during *in vitro* PAT imaging

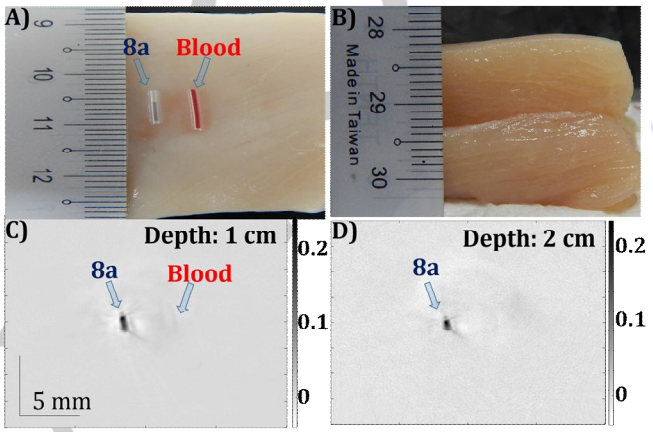

Figure 7. Deep tissue cross-sectional photoacoustic tomography (PAT) imaging of aza-BODIPY dye, **8a** and blood embedded inside chicken breast tissue using OPO-PAT system. (A) LDPE tubes filled with **8a** and blood. (B) Layers of chicken tissue in stacks inside which blood and **8a** were placed. (C) Cross-sectional PAT image at 1 cm depth. (D) Cross-sectional PAT image at 2 cm depth.

Conclusion

In conclusion, we have designed and synthesized four novel *N*-ethylcarbazole linked aza-BODIPY dyes and investigated their efficiency to produce triplet excited state and singlet oxygen generation. All these aza-BODIPY derivatives showed strong absorption in the NIR region with high molar extinction coefficients (3-4x10^4 $M^{-1}cm^{-1}$). The substitution of these derivatives with heavy atoms such as iodine at the core positions resulted in a significant enhancement in the intersystem crossing efficiency of 9a-b. The triplet excited state quantum yields of *ca*. 90% and singlet oxygen generation efficiency of *ca*. 70% were observed for the core iodinated derivative **9a**. The orientation of carbazole group and the localisation of electron density in the molecule were confirmed from the optimised geometries through DFT calculations. Strong photoacoustic signal observed in the NIR region makes these molecules ideal for deep tissue contrast agent for photoacoustic imaging. Up to 2 cm deep photoacoustic imaging was successfully demonstrated by using **8a** as contrast agent. Our results demonstrate that these derivatives can have potential for theranostic application of simultaneous imaging and therapy by combining both photoacoustic imaging and photodynamic therapy.

Accepted Manuscript

This article is protected by copyright. All rights reserved.

Experimental Section

General Techniques: The melting points were determined on a µThermoCal10 apparatus. The electronic absorption spectra were recorded on a Shimadzu UV-3101 or 2401 PC UV-VIS-NIR scanning spectrophotometer. The fluorescence spectra were recorded on a SPEX-Fluorolog F112X spectrofluorimeter. ^{1}H, ^{13}C, ^{11}B and ^{19}F NMR (Fig. S1-S22, Supporting Information) were recorded on a 500 MHz Agilent NMR VNMRS spectrometer. Mass spectra were recorded on Bruker (maxis impact), sr. no. 282001.00081. All the solvents used were purified and distilled before use. Fluorescence quantum yields were measured by the integration of the available area of fluorescence spectra by absolute method using an integration sphere. Tris-(8-hydroxyquinoline)aluminium (Alq_3) was used for the calibration of integration sphere before starting the experiments.[21]

Quantification of triplet state properties: The nanosecond laser flash photolysis experiments were carried out by employing an Applied Photophysics model LKS-20 laser kinetic spectrometer using OCR-12 Series Quanta Ray Nd:YAG laser. Laser beams were fixed at right angles to each other. The laser energy was 64 mJ at 355 nm. The triplet yields (Φ_T) of the synthesized aza-BODIPYs were measured employing energy transfer to β-carotene using $Ru(bpy)_3^{2+}$as the reference.[12] For these experiments, an optically matched (355 nm) solutions of $Ru(bpy)_3^{2+}$/aza-BODIPY derivatives were mixed with a known volume of β-carotene solution (end concentration of β-carotene was 2.0×10^{-4} M). The transient absorbance (ΔA) of the β-carotene triplet, formed by the energy transfer from $Ru(bpy)_3^{2+}$ or the aza-BODIPY triplet, was monitored at 510 nm. The plateau absorbance following the completion of triplet formation were compared and properly corrected for the decay of the donor triplets in competition with energy transfer to β -carotene, and thus calculated the Φ_T of aza-BODIPY derivatives based on eq. 1.

$$\Phi_T^{bod} = \Phi_T^{ref} \frac{\Delta A_{bod}}{\Delta A_{ref}} \frac{k_{obs}^{bod}}{k_{obs}^{bod} - k_0^{bod}} \frac{k_{obs}^{ref} - k_0^{ref}}{k_{obs}^{ref}} \quad \ldots\ldots\ldots \text{(eq. 1)}$$

where superscripts 'bod' and 'ref' designate the different aza-BODIPY derivatives and $Ru(bpy)_3^{2+}$, respectively, k_{obs}, is the pseudo-first-order rate constant for the growth of the β-carotene triplet and k0 is the rate constant for the decay of the donor triplets, in the absence of β-carotene, observed in solutions containing $Ru(bpy)_3^{2+}$ or aza-BODIPY dye at the same optical density (OD) as those used for sensitization. The direct excitation of β-carotene did not result in any significant triplet formation under these experimental conditions, because of negligible triplet yield. The Φ_T^{ref} in methanol for $Ru(bpy)_3^{2+}$ was taken to be unity. The Φ_T data obtained in this manner are reliable to the extent to which the assumption regarding 100% efficiency of energy transfer to β-carotene is valid.

Quantification of singlet oxygen generation: Singlet oxygen generation studies were carried out with a light source 200 W mercury lamp (model 3767) on an Oriel optical bench (model 11200) with a grating monochromator (model 77250). The intensity of light was maintained constant throughout the irradiations by measuring the output using an Oriel photodiode detection system (model 7072). Quantum yields for singlet oxygen generation in DMSO were determined by monitoring the photooxidation of DPBF sensitized by the aza-BODIPY derivatives. Singlet oxygen quantum yields were measured at low dye concentrations (optical density 0.2-0.3 at the irradiation wavelengths >630 nm) to minimize the possibility of singlet oxygen quenching by the dyes. The photooxidation of DPBF was monitored between 2 s to 2 min. depending on the efficiency of the dye sensitizer. No thermal recovery of DPBF (from a possible decomposition of endoperoxide product) was observed under the conditions of these experiments. The quantum yields of singlet oxygen generation ($\Phi[^1O_2]$) were calculated by a relative method using optically matched solutions and comparing the quantum yield of photooxidation of DPBF sensitized by the dye of interest to the quantum yield of **MB** ($\Phi[^1O_2]$ = 52%) as the reference.[14] The following eq. 2 was used,

$$\Phi\Delta^{bod} = \Phi\Delta^{MB} \frac{m^{bod}}{m^{MB}} \frac{F^{MB}}{F^{bod}} \ldots\ldots \text{(eq. 2)}$$

where superscripts 'bod' and 'MB' designate aza-BODIPY derivatives and MB, respectively, $\Phi\Delta$ is the quantum yield of singlet oxygen, 'm' is the slope of a plot of difference in change in absorbance of DPBF (at 418 nm) with the irradiation time and 'F' is the absorption correction factor, which is given by $F = 1 - 10^{-OD}$ (OD at the irradiation wavelength).

Photoacoustic imaging system: Each sample was injected into a transparent LDPE tube of 0.38 mm inner diameter and was irradiated with Optical Parametric Oscillator (OPO) laser (Continuum, Surelite) pumped with 10 Hz repetition rate Q-switched Nd:YAG laser maintaining 5 ns pulse width and pulse energy density of ~5-10 mJ/cm^2. The laser irradiation results in thermoelastic expansion of the sample which in turn generates PA waves. These PA waves are detected using a single-element UST (Olympus NDT, V306-SU) of 2.25 MHz central frequency with ~70% nominal bandwidth. The UST and the LDPE tubes were enclosed in a water bath for better acoustic coupling. The acquired PA signal was first amplified and band pass filtered (1-10 MHz) using a pulse amplifier (Olympus-NDT, 5072PR) and then recorded using a data acquisition card (GaGe, compuscope 4227) inside a desktop. All PA signals were acquired with a sampling rate of 25 MHz. The laser wavelength was varied from 670-970 nm with step size of 5 nm. Each PA signal was averaged 10 times and normalised with laser power and amplifier gain.For deep tissue imaging experiments, we have used the OPO-PAT system (Fig 1. in [19]). The PA signal was acquired by rotating the UST continuously in a full 360^0 around the sample. The acquired PA data was then amplified and filtered. A simple delay-and-sum reconstruction algorithm was used to obtain the PAT images.[20] SNR of the PAT images were calculated as the ratio of peak-to-peak amplitude of the PA signal (*V*) to the standard deviation of background noise (*n*) *i.e. SNR (in dB) = 20 log$_{10}$ (V/n).*

Materials and Methods: The starting materials. carbazole, acetophenone, 4-bromoacetophenone, ethyl iodide, nitromethane, diethylamine, ammonium acetate, borontrifluoride diethyl etherate, triethylamine, *N*-iodosuccinimide, methylene blue, 1,3-diphenylisobenzofuran, β-carotene were purchased from S. D. Fine and sigma Aldrich Chemicals, India.1,3-diphenylisobenzofuran (DPBF) was recrystallized from a mixture (1:1) of ethanol and chloroform. The compounds **2** (mp: 71-73^{0}C) and **3** (mp: 85-87^{0}C) were synthesized in good yields by following the literature reported procedures.[22]

*General procedure for the synthesis of **5a-b***

5a-b were synthesized by modifying the reported procedures [22a, 23], 9-ethyl-9H-carbazole-3-carbaldehyde, **2** (0.022 mol) and acetophenone derivatives **3a-b** (0.022 mol) were dissolved in methanol (300 mL) and 2.5 molar aq. KOH (150 ml) added dropwise while cooling. After the complete addition, reaction mixture allowed to stir for 24 h. The precipitated product was filtered, washed with cold methanol, dried and recrystallized from ethanol to give **5a-b** as yellow solid.

5a: 63%, mp 67-69 °C; ^1H NMR (500 MHz, $CDCl_3$) δ 8.17 (m, 1H), 8.04 (d, J = 7.5 Hz, 1H), 7.92 (d, J = 8.0 Hz, 2H), 7.53 – 7.49 (m, 2H), 7.39-7.36 (dd, J=8.2 1H), 7.18 – 7.10 (m, 4H), 7.06-7.04 (m, 2H), 7.00 (d, 1H),

This article is protected by copyright. All rights reserved.

4.25 (q, J=7.2 Hz 2H), 1.14 (t, J = 7.1 Hz, 3H). ^{13}C NMR (125 MHz, $CDCl_3$) 189.04, 146.50, 142.34, 140.83, 139.57, 135.92, 130.28, 125.65, 124.31, 122.67, 121.04, 119.8, 118.4, 113.08, 111.44, 110.47, 109.0, 108.60, 47.10, 38.80, 15.19 cm^{-1}; ESI-MS m/z Cald for $C_{23}H_{19}NO$ 325.147, Found 326.02.

5b: 58%, mp 125-127 °C; ^{1}H NMR (500 MHz, $CDCl_3$) δ 8.38 (s, 1H), 8.15 (d, J = 7.6 Hz, 1H), 8.06 (d, J = 15.5 Hz, 1H), 7.94 (d, J = 8.4 Hz, 2H), 7.79 (d, J = 8.5 Hz, 1H), 7.66 (d, J = 8.4 Hz, 2H), 7.53 (dd, J = 15.3, 6.0 Hz, 2H), 7.46 – 7.41 (m, 2H), 7.30 (m, 1H), 4.40 (q, J = 7.3 Hz, 2H), 1.47 (t, J = 7.2 Hz, 3H). ^{1}H NMR (126 MHz, $CDCl_3$) δ; 189.46, 147.13, 141.59, 140.51, 137.52, 131.84, 129.98, 127.40, 125.70, 123.51, 122.78, 121.78, 120.67, 119.82, 118.38, 109.13, 108.93, 108.17, 37.81, 13.85 cm^{-1}; ESI-MS m/z Cald for $C_{23}H_{18}BrNO$ 403.057, Found 404.06.

*General procedure for the synthesis of **6a-b***

6a-b were synthesized by modifying the reported procedures [24, 3a] To a solution of **5a-b** (0.02 mol) dissolved in 100 mL of methanol was added diethyl amine (9 mL) and nitromethane (4.5 mL) and refluxed for 24 h. The mixture was cooled and neutralized using 1N HCl and extracted with chloroform. The removal of the solvent gave a residue which was separated by column chromatography over silica gel. Elution of the column with a mixture (1:9) of ethyl acetate and hexane gave **6a-b** in good yields.

6a: 69%, Viscous liquid; 1H NMR (500 MHz, $CDCl_3$) δ 8.46 (m, J = 8.4 Hz, 2H), 7.97 (m, 1H), 7.82 (m, 1H), 7.69 (m, 2H), 7.62 (m, 1H), 7.46 (m, 2H), 7.29 (m, 2H), 7.08 (m, 1H) 4.87 (m, 2H), 4.75 (m, 2H), 4.19 (m, 1H), 2.97 (d, 2H), 1.44 (t, J = 7.2 Hz, 3H); ^{13}C NMR (126 MHz, $CDCl_3$) δ 196.56, 163,41 139.21, 137.72, 133.50, 131.67, 129.51, 129.09, 127.89, 126.93, 125.15, 124.78, 122.78, 121.04, 118.19, 118.08, 80.46, 42.21, 39.46, 37.56, 36.51, 31.3, 30.48, 13.76; ESI-MS m/z Cald for $C_{24}H_{22}N_2O_3$ 386.163, Found 387.1

6b: 80%, m.p. 69-71 °C; 1H NMR (500 MHz, $CDCl_3$) δ 8.03 (dd, J = 7.4 Hz, 2H), 7.69 (dd, J = 8.6 Hz, 2H), 7.47 (m, 1H), 7.39 (m, 1H), 7.29 (m, 2H), 7.08 (m, 1H), 4.80 (m, 1H), 4.41 (m, 2H), 3.56 (m, 2H), 2.92 (d, 2H), 1.42 (t, J = 7.2 Hz, 3H); ^{13}C NMR (126 MHz, $CDCl_3$) δ 196.34, 163.0, 140.28, 139.40, 135.30, 132.06, 129.54, 129.04, 128.70, 126.01, 124.88, 123.30, 122.41, 120.46, 119.15, 118.95, 80.42, 42.19, 39.55, 37.60, 36.47, 31.42, 30.48, 13.83; ESI-MS m/z Cald for $C_{24}H_{21}BrN_2O_3$ 464.074, Found 465.0.

*General Procedure for the synthesis of **7a-b***

The nitromethane derivatives **6a-b** (0.01 mol) and ammonium acetate (27.30 g, 0.314 mol) were dissolved in n-butanol (60 mL) and heated under reflux for 24 h.[15c] The precipitated product was filtered, washed with cold ethanol, dried and recrystallized from chloroform to give **7a-b** as brown solid.

7a: 57%, m.p. 225-227 °C; ^{1}H NMR (500 MHz, $CDCl_3$) δ 8.84 (s, 2H), 8.33 (d, J = 8.5 Hz, 2H), 8.02 (d, J = 7.3 Hz, 4H), 7.86 (d, J = 7.6 Hz, 2H), 7.55 (t, J = 7.6 Hz, 4H), 7.47 (t, J = 7.3 Hz, 2H), 7.39 (m, 4H), 7.31 (d, J = 8.5 Hz, 2H), 7.27 (s, 2H), 7.01 (t, J = 7.3 Hz, 2H), 4.27 (q, J = 7.2 Hz, 4H), 1.38 (t, J = 7.2 Hz, 6H); ^{13}C NMR (126 MHz, $CDCl_3$) δ 154.79, 149.83, 143.80, 140.26, 139.83, 132.57, 129.70, 129.04, 127.21, 126.51, 125.47, 125.20, 123.36, 123.20, 121.48, 120.77, 118.71, 113.37, 108.52, 108.37, 77.24, 76.99, 76.74, 37.58, 13.87; ESI-MS m/z Cald for $C_{48}H_{37}N_5$ 683.305, Found 684.312.

7b: 66%, m.p. 272-274 °C;.^{1}H NMR (500 MHz, $CDCl_3$) δ 8.58 (s, 2H), 8.13 (d, *J* = 7.6 Hz, 2H), 8.10 (d, *J* = 7.8 Hz, 4H), 7.50 (d, *J* = 7.3 Hz, 2H), 7.46 (m, 4H), 7.43 (d, 2H), 7.42 – 7.39 (m, 4H), 7.35 (m, 2H), 7.26 (s, 1H), 7.19 (t, *J* = 7.4 Hz, 2H), 4.31 (q, *J* = 7.3 Hz, 4H), 1.46 (t, *J* = 7.3 Hz, 6H). ^{13}C NMR (126 MHz, $CDCl_3$) δ 154.76, 149.49, 141.50, 140.97, 140.47, 134.18, 128.98, 128.11, 127.51, 126.16, 124.62, 123.59, 123.35, 123.01, 120.64, 119.47, 118.86, 114.09, 108.95, 108.86, 37.70, 13.89; ESI-MS m/z Cald for $C_{48}H_{35}Br_2N_5$ 841.124, Found 842.0.

*General procedure for the synthesis of **8a-b***

8a-b were synthesized by modifying the reported procedures.[25, 15c] Compounds **7a-b** (0.62 mmol) dissolved in dry dichloromethane (100 mL) was treated with triethylamine (1.14 mL, 8.1 mmol) and stirred for 10 min at 30°C. To this reaction mixture, boron trifluoride diethyl etherate (4.65 mL, 13.1 mmol) was added and heated at 40°C for 5 h. The solvent was evaporated, washed with water (2 × 50 mL) and extracted with chloroform. Removal of the solvent gave a residue, which was separated by column chromatography over silica gel. Elution of the column with a mixture (1:9) of ethyl acetate and hexane gave the products **8a-b** as metallic blue solid.

8a: 34%, m.p. 234-236°C; ^{1}H NMR (500 MHz, DMSO) δ 9.06 (s, 2H), 8.47 (d, *J* = 8.7 Hz, 2H), 8.12 (m, 4H), 8.07 (d, *J* = 7.7 Hz, 2H), 7.66 (m, 6H), 7.57 (m, 6H), 7.47 (m, 2H), 7.12 (m, 2H), 4.44 (m, 4H), 1.31 (t, *J* = 7.1 Hz, 6H). ^{13}C NMR (126 MHz, DMSO) δ 158.59, 145.78, 145.01, 140.76, 140.42, 132.18, 130.38, 129.49, 128.45, 128.00, 127.44, 126.03, 124.03, 123.64, 123.32, 122.21, 120.88, 119.25, 117.18, 108.97, 108.73, 37.74, 13.95. ^{11}B NMR (160 MHz, DMSO) δ 1.22, 1.02, 0.83. ^{19}F NMR (470 MHz, DMSO) δ -128.40, -128.47, -128.54, -128.61; ESI-MS m/z Cald for $C_{48}H_{36}BF_2N_5$ 731.303, Found 732.310.

8b: 41%, m.p. 289-291 °C; ^{1}H NMR (500 MHz, DMSO) δ 9.06 (d, 2H), 8.47 (d, *J* = 8.5 Hz, 2H), 8.30 (s, 2H), 8.04 (m, 6H), 7.79 (m, 3H), 7.68 (m, 4H), 7.48 (m, 3H), 7.12 (m, 2H), 4.45 (m, 4H), 1.31 (d, *J* = 7.2 Hz, 6H); ^{13}C NMR (126 MHz, DMSO) δ 158.40, 145.46, 145.03, 140.94, 140.55, 131.89, 131.29, 129.80, 129.07, 127.80, 126.81, 123.66, 123.39, 122.88, 122.56, 121.02, 119.85, 118.57, 110.13, 37.69, 14.33. ^{19}F NMR (470 MHz, DMSO) δ -128.28, -128.34, -128.41, -128.48; ESI-MS m/z Cald for $C_{48}H_{34}BBr_2F_2N_5$ 889.122, Found 890.130.

*General procedure for the synthesis of **9a-b***

To a solution of **8a-b** (0.27 mmol) in a mixture (60 mL, 3:1) of chloroform and acetic acid, *N*-iodosuccinimide (154 mg, 0.68 mmol) was added and stirred at 30°C for 2 h. The reaction mixture was washed with sodium thiosulphate followed by sodium bicarbonate solution and extracted with chloroform. Removal of the solvent gave a residue which was separated by column chromatography over silica gel. Elution of the column with a mixture (1:9) of methanol and chloroform gave 60-65% of **9a-b**.

9a: 61%, m.p. >300 °C; ^{1}H NMR (500 MHz, DMSO) δ 8.69 (d, 2H), 8.61 (m, 2H), 8.14 (m, 2H), 8.08 (d, *J* = 8.4 Hz, 1H), 7.97 (d, *J* = 9.0 Hz, 1H), 7.76 (m, 2H), 7.59 (m, 4H), 7.53 (m, 6H), 7.48 (m, 2H), 7.43 (m, 2H), 4.30 (m, 4H), 1.06 (t, *J* = 7.1 Hz, 6H); ^{13}C NMR (126 MHz, DMSO) δ 158.40, 145.46, 145.03, 140.94, 140.55, 131.89, 131.29, 129.80, 129.07, 127.80, 126.81, 123.66, 123.39, 122.88, 122.56, 121.02, 119.85, 118.57, 110.13, 37.69, 14.33; ^{19}F NMR (470 MHz, DMSO) δ -130.01, -130.08, -130.13, -130.18; ESI-MS m/z Cald for $C_{48}H_{34}BF_2I_2N_5$ 983.096, Found 984.033.

9b: 58%, m.p. >300 °C; ^{1}H NMR (500 MHz, $CDCl_3$) δ 8.59 (s, 1H), 8.53 (s, 1H), 8.48 (s, 1H), 8.17 (d, 2H), 8.10 – 8.08 (m, 2H), 7.85 (m, 1H), 7.77

Accepted Manuscript

This article is protected by copyright. All rights reserved.

(m, 1H), 7.66 (m, 1H), 7.59 (m, 6H), 7.30 (m, 4H), 7.05 (m, 2H), 4.15(m, 4H), 0.85 (s, 6H). ^{11}B NMR (160 MHz, $CDCl_3$) δ 0.38, 0.23, 0.03. ^{19}F NMR (470 MHz, $CDCl_3$) δ -131.69, -131.75, -131.81, -131.87; ESI-MS m/z Cald for $C_{48}H_{32}BBr_2F_2I_2N_5$ 1140.915, Found 1141.925.

Acknowledgements

The authors Y. G. and N. S. greatly thankful to University Grant Commission-SAP, New Delhi, India for providing financial support. The authors N. A, J. J and D. R acknowledge the financial support from CSIR(CSC0134&NWP55), and Department of Science and Technology, Government of India. Author M. P. Acknowledges the finantial support by the Tier 1 grant funded by the Ministry of Education in Singapore (RG41/14: M4011285, RG48/16: M4011617), and the Singapore Ministry of Health's National Medical Research Council (NMRC/OFIRG/0005/2016: M4062012). Authors have no relevant financial interests in the manuscript and no other potential conflicts of interest to disclose.

Keywords: Aza-BODIPY • Dyes and pigments • Triplet excited state • Singlet oxygen • Photoacoustic spectra

References

[1] a) S. Toyokuni, *Pathol. Int.* **1999**, *49*, 91–102; b) S. G. Awuah, Y. You, *RSC Adv.* **2012**, *2*, 11169.

[2] a) C. Schweitzer, R. Schmidt, *Chem. Rev.* **2003**, *103*,1685−1757; b) E. S. Nyman, H. Hynninen, *J. Photochem. Photobiol. B* **2004**, *73*, 1–28; c) I. S. Turan, D. Yildiz, A.Turksoy, G. Gunaydin, E. U. Akkaya, *Angew. Chem. Int. Ed.* **2016**, *55*, 2875–2878; d) S. D. Topel, G. T. Cin, E. U. Akkaya, *Chem. Commun.* **2014**, *50*, 8896–8899.

[3] a) N. Adarsh, M. Shanmugasundaram, R. R. Avirah, D. Ramaiah, *Chem. Eur. J.* **2012**, *18*, 12655–12662; b) V. S. Thoi, J. R. Stork, D. Magde, S. M. Cohen, *Inorg. Chem.* **2006**, *45*, 10688–10697; c) I. S. Turan, F. P. Cakmak, D. C. Yildirim, R. Cetin-Atalay, E. U. Akkaya, *Chem. Eur. J.* **2014**, *20*, 16088–16092.

[4] a) T. Matsubara, K. Kusuzaki, A. Matsumine, H. Satonaka, K. Shintani, T. Nakamura, A. Uchida, *In Vivo.* **2008**, *22*, 297–304; b) C. W. Lin, J. R. Shulok, S. D. Kirley, C. M. Bachelder, T. J. Flotte, M. E. Sherwood, L. Cincotta, J. W. Foley, *Photochem. Photobiol.* **1993**, *58*, 81–91; c) C. W. Lin, J. R. Shulok, S. D. Kirley, L. Cincotta, J. W. Foley, *Cancer Res.* **1991**, *51*, 2710–2719; d) R. Danaboyina, A. Joy, N. Chandrasekhar, N. V Eldho, S. Das, M. V George, *Photochem. Photobiol.* **1997**, *65*, 783–790; e) K. Jyothish, R. R. Avirah, D. Ramaiah, *Org. Lett.* **2006**, *8*, 111–114; f) R. R. Avirah, D. T. Jayaram, N. Adarsh, D. Ramaiah, *Org. Biomol. Chem.* **2012**, *10*, 911.

[5] a) P. Agostinis, K. Berg, K. A. Cengel, T. H. Foster, A. W. Girotti, S. O. Gollnick, S. M. Hahn, M. R. Hamblin, A. Juzeniene, D. Kessel, *Am. Cancer Soc.* **2011**, *61*, 250–281; b) S. Erbas-Cakmak, F. P. Cakmak, S. D. Topel, T. B. Uyar, E. U. Akkaya, *Chem. commun.* **2015**, *51*, 12258–61.

[6] a) A. Kamkaew, S. H. Lim, H. B. Lee, L. V. Kiew, L. Y. Chung, K. Burgess, *Chem. Soc. Rev.* **2013**, *42*, 77–88; b) T. Yogo, Y. Urano, Y. Ishitsuka, F. Maniwa, T. Nagano, *J. Am. Chem. Soc.* **2005**, *127*, 12162–12163; c) P. Batat, M. Cantuel, G. Jonusauskas, L. Scarpantonio, A. Palma, D. F. O'Shea, N. D. McClenaghan, *J. Phys. Chem. A* **2011**, *115*, 14034–14039. d) N. Adarsh, R. R. Avirah, D. Ramaiah *Org. Lett.* **2010**, *12*, 5720–5723; e) J. K. G. Karlsson, A. Harriman, *J. Phys. Chem. A* **2016**, *120*, 2537–2546; f) A. Nano, P. Retailleau, J. P. Hagon, A. Harriman, R. Ziessel, *Phys. Chem. Chem. Phys.* **2014**, *16*, 10187–98; g) R. Misra, T. Jadhav, B. Dhokale, P. Gautam, R. Sharma, R. Maragani, S. M. Mobin, *Dalton Trans.* **2014**, *43*, 13076; h) A. Harriman, P. Stachelek, A. Sutter, R. Ziessel, D. Beljonne, C. Curutchet, G. D. Scholes, R. J. Silbey, J. S. Wu, W. M. Liu, et al., *Photochem. Photobiol. Sci.* **2015**, *14*, 1100–1109.

[7] a) W. M. Gallagher, L. T. Allen, C. O'Shea, T. Kenna, M. J. Hall, J. Killoran, D. F. O'Shea, *Br. J. Cancer* **2005**, *92*, 1702-1710; b) A. T. Byrne, A. E. O'Connor, M. Hall, J. Murtagh, K. O'Neill, K. M. Curran, K. Mongrain, J. A. Rousseau, R. Lecomte, S. McGee, J. J. Callanan, D. F. O'Shea, W. M. Gallagher, *Br. J. Cancer* **2009**, *101*, 1565-1573; c) J. Joseph, N. V. Eldho, D. Ramaiah, *Chem. Eur. J.* **2003**, *9*, 5926–5935; d) S. Kumar, T. K. Khan, M. Ravikanth, *Tetrahedron* **2015**, *71*, 7608–7613; e) A. Dvivedi, S. Kumar, M. Ravikanth, *Sens. Actuators, B.* **2016**, *224*, 364–371; f) S. Kumar, H. B. Gobeze, T. Chatterjee, F. D'Souza, M. Ravikanth, *J Phys. Chem. A* **2015**, *119*, 8338–8348; g) R. Sharma, H. B. Gobeze, F. D'Souza, M. Ravikanth, *ChemPhysChem* **2016**, *5017*, 2516–2524; h) T. Jadhav, R. Misra, S. Biswas, G. D. Sharma, *Phys. Chem. Chem. Phys.* **2015**, *17*, 26580–26588; i) N. Balsukuri, M. Y. Lone, P. C. Jha, S. Mori, I. Gupta, *Chem. Asian J.* **2016**, *11*, 1572–1587.

[8] S. Huang, P. K. Upputuri, H. Liu, M. Pramanik, M. Wang, *J. Mater. Chem. B* **2016**, *4*, 1696–1703.

[9] a) L. V. Wang, S. Hu, *Science* **2012**, *335*, 1458–1462; b) L. V Wang, J. Yao, *Nat. Methods.* **2016**, *13*, 627–638. c) W. Xia, D. Piras, M. K. A. Singh, J. C. G. van Hespen, T. G. van Leeuwen, W. Steenbergen, S. Manohar, *Biomed. Opt. Express* **2013**, *4*, 2555–69; d) C. Kim, J. A. Margenthaler, M. D. Pashley, L. V Wang, *radiology* **2010**, *256*, 102–110; e) M. Pramanik, G. Ku, C. Li, L. V. Wang, *Med. Phys.* **2008**, *35*, 2218–2223. e) X. Cai, C. Kim, M. Pramanik, L. V Wang, *J. Biomed. Opt.* **2011**, *16*, 46017.

[10] a) D. Pan, M. Pramanik, A. Senpan, J. S. Allen, H. Zhang, S. a Wickline, L. V Wang, G. M. Lanza, *The FASEB J.* **2011**, *25*, 875–882; b) M. Pramanik, K. H. Song, M. Swierczewska, D. Green, B. Sitharaman, L. V Wang, *Phys. Med. Biol.* **2009**, *54*, 3291–301; c) A. De la Zerda, C. Zavaleta, S. Keren, S. Vaithilingam, S. Bodapati, Z. Liu, J. Levi, B. R. Smith, T.-J. Ma, O. Oralkan, Z. Cheng, X. Chen, H. Dai, B. T. Khuri-Yakub, and S. S. Gambhir, *Nat. Nanotechnol.* **2008**,*3*(9), 557-562; d) C. Kim, C. Favazza, and L. V. Wang, *Chem. Rev.* **2010,***110*(5), 2756-2782; e) K. Sivasubramanian, M. Mathiyazhakan, C. Wiraja, P. K. Upputuri, C. Xu, and M. Pramanik, *J. Biomed. Opt.* **2017** *22* (4), (In Press); f) Y. Toumia, F.Domenici, S. Orlanducci, F. Mura, D. Grishenkov, P. Trochet, S. Lacerenza, F. Bordi, and G. Paradossi, *ACS Appl. Mater. Interfaces* **2016**, *8*, (25) 16465. g) Y. Shi, D. Peng, K. Wang, X. Chai, Q. Ren, J. Tian, and C. Zhou, *Biomed. Opt. Express* **2017,** *7*, 1830-1841; h) C. Gao, Z.-J. Deng, D. Peng, Y.-S. Jin, Y. Ma, Y.-Y. Li, Y.-K. Zhu, J.-Z. Xi, J. Tian, and Z.-F. Dai, *Cancer Biology & Medicine* **2016** *13* (3), 349-359; i) K. Pu, A. J. Shuhendler, J. V. Jokerst, J. Mei, S. S. Gambhir, Z. Bao, and J. Rao, *Nat. Nanotechnol.* **2014** *9* (3), 233-239.

[11] a) D. Ramaiah, A. Joy, N. Chandrasekhar, N. V. Eldho, S. Das, M. V. George, *Photochem. Photobiol.***1997**, *65*, 783–790.

[12] a) V. S. Jisha, K. T. Arun, M. Hariharan, D. Ramaiah, *J. Phys. Chem. B* **2010**, *114*, 5912–5919.

[13] M. Mirenda, C. A. Strassert, L. E. Dicello,San Roman E. *ACS Appl. Mater. Interfaces* **2010**, *2*, 1556–1560.

[14] a) P. R. Ogilby, C. S. Foote, *J. Am. Chem. Soc.***1983**, *105*, 3423–3430; b) M. Nemoto, H. Kokubun, M. Koizumi, *Bull. Chem. Soc.* **1969**, *42*, 1223–1228

[15] a) R. R. Gagne, C. A. Koval, G. C. Lisensky, *Inorg. Chem.* **1980**, *19*, 2854–2855; b) P. E. Kesavan, I. Gupta, *Dalt. Trans.* **2014**, *43*, 12405–12413; c) A. Gorman, J. Killoran, C. O'Shea, T. Kenna W. M. Gallagher, D. F. O'Shea, *J. Am. Chem. Soc.* **2004**, *126* 10619–10631.

[16] T. Le Bahers, C. Adamo, F. Odobel, D. Jacquemin, *J. Phys. Chem. C* **2012**,*116*, 11946–11955.

[17] M. D. Kasha, *Faraday Soc.***1950**, *9*, 14−19.

[18] M. Frenette, M. Hatamimoslehabadi, S. Bellinger-buckley, S. Laoui, J. La, S. Bag, S. Mallidi, T. Hasan, B. Bouma, C. Yelleswarapu, J. Rochford, *J. Am. Chem. Soc.* **2014**, *136*, 15853−15856.

[19] P. K. Upputuri, and M. Pramanik, *Biomedical Optics Express,* **2015** *6* (10), 4118-4129.

[20] S. K. Kalva, and M. Pramanik, *J. Biomed. Opt.* **2016** *21* (8), 086011.

[21] L. D. Carlos, C. De Mello Donegá, R. Q. Albuquerque, S. Alves, J. F. S. Menezes, O. L. Malta, *Mol. Phys.* **2003**, *101*, 1037–1045

[22] a) G. Bai, J. Li, D. Li, C. Dong, X. Han, P. Lin, *Dye. Pigment.* **2007**, *75*, 93–98. b) K. G. Thorat, P. Kamble, A. K. Ray, N. Sekar, *Phys. Chem. Chem. Phys.* **2015**, *17*, 17221–17236

[23] V. D. Gupta, V. S. Padalkar, K. R. Phatangare, V. S. Patil, P. G. Umape, N. Sekar, *Dye. Pigment* **2011**, *88*, 378–384.

[24] S. C. Lee, D. Zhai, P. Mukherjee, Y. T. Chang, *Mater.* **2013**, *6*, 1779–1788.

[25] P. A. Bouit, K. Kamada, P. Feneyrou, G. Berginc, L. Toupet, O. Maury, C. Andraud, *ADV MATER* **2009**, *21*, 1151–1154.

Accepted Manuscript

This article is protected by copyright. All rights reserved.

10.1002/chem.201605702

WILEY-VCH

Table of Contents

FULL PAPER

The carbazole linked aza-BODIPY dyes showed favorable photophysical properties and efficient triplet as well as singlet oxygen generation quantum yields. Furthermore, the efficient photoacoustic signals produced by these dyes makes them as excellent candidates for both photodynamic therapy and contrast agents for photoacoustic imaging.

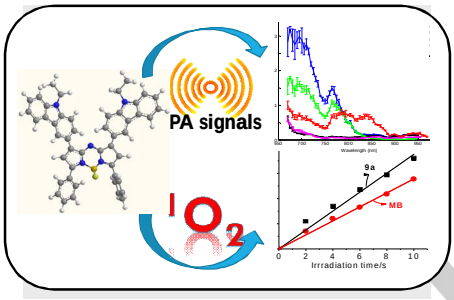

Y. Gawale, N. Adarsh, S. K. Kalva, J. Joseph, M. Pramanik, D. Ramaiah* and N. Sekar**

xxxxx – xxxxx

Carbazole Linked NIR Aza-BODIPY Dyes as Triplet Sensitizers and Photoacoustic Contrast Agents for Deep Tissue Imaging

WILEY-VCH Accepted Manuscript

This article is protected by copyright. All rights reserved.